

Table 1: Summary of allocation request. The physics packages used in each project and adaptive mesh refinement (AMR) structure are described in Sections 2 and 3. The total node hours and disk usage are described in Section 4.

Name	Node Hours	Disk	Physics	AMR
Turbulence	$4.5 \times 10^4$	$5.6 \times 10^3$	Hydro + Driving	None
Cores	$1.1 \times 10^3$	$2.0 \times 10^4$	MHD + Gravity + Particles	4 levels, all space
CMB	$2.6 \times 10^4$	$1.7 \times 10^4$	MHD + Driving	None
Galaxies	$2.2 \times 10^5$	$2.2 \times 10^4$	MHD + Gravity + Cooling	8 level nest
	$2.9 \times 10^5$	$6.4 \times 10^4$		

## Four Projects in Astrophysical Magnetohydrodynamics

**PI: David C. Collins** (Florida State University)

### 1 Introduction

We are requesting  $1.6 \times 10^5$  SUs on Stampede 2 for the period beginning June 1, 2022. This allocation will support four projects involving astrophysical magnetic fields and turbulence. The first project (*turbulence*) explores analytical formulae we have developed for isothermal turbulence, which is relevant for many astrophysical processes, among them the formation of stars. The second project (*cores*) examines fractal structures in star forming clouds. The third project (*foregrounds*) examines the polarized signal produced by the interstellar medium, which is in the foreground of our understanding of the distant cosmic microwave background (CMB). The fourth project (*galaxies*) simulates entire galaxies, in order to understand the growth of the magnetic field. This research is supported by two NSF grants. The first two projects (*turbulence* and *cores*) are supported by NSF AST-1616026, and the third (*foregrounds*) is supported by NSF AST-2009870. We are hopeful that the *galaxies* project will be funded by a pending proposal.

These projects support three graduate students. Luz Jimenez Vela is working on the *cores* project; Branislav Rabatin is working on the *turbulence* and *foregrounds* projects; and Jacob Strack is working on the *galaxies* project.

Table 1 shows the cost for each project. Each of the four projects uses a slightly different physics package, which affects the cost of the simulation. In addition, two of the four projects employ adaptive mesh refinement (AMR), a technique that adaptively changes the resolution of the simulation. This also affects the cost of the simulation. We motivate each project and describe the simulations to be run in Section 2. In Section 3 we describe the computational tools to be used. In Section 4 we give the projected cost and disk usage of these simulations.

### 2 Scientific Background

Here we will introduce the physical motivation for the projects, and describe the simulations to be performed. Detailed accounting of the cost can be found in Section 4, and performance details can be found in the Scaling document.

#### 2.1 Background: Turbulent Energy

Turbulence is ubiquitous in astrophysical processes. We have developed analytic predictions for the distribution of energies in isothermal turbulence, both supersonic and subsonic. These simulations will verify our analytic predictions, and examine if deviations seen in preliminary studies are due to lack of resolution or interesting physics. We provide the background for the *turbulence* project in Section 2.1.1, and motivate the simulations that support this study in Section 2.1.2.

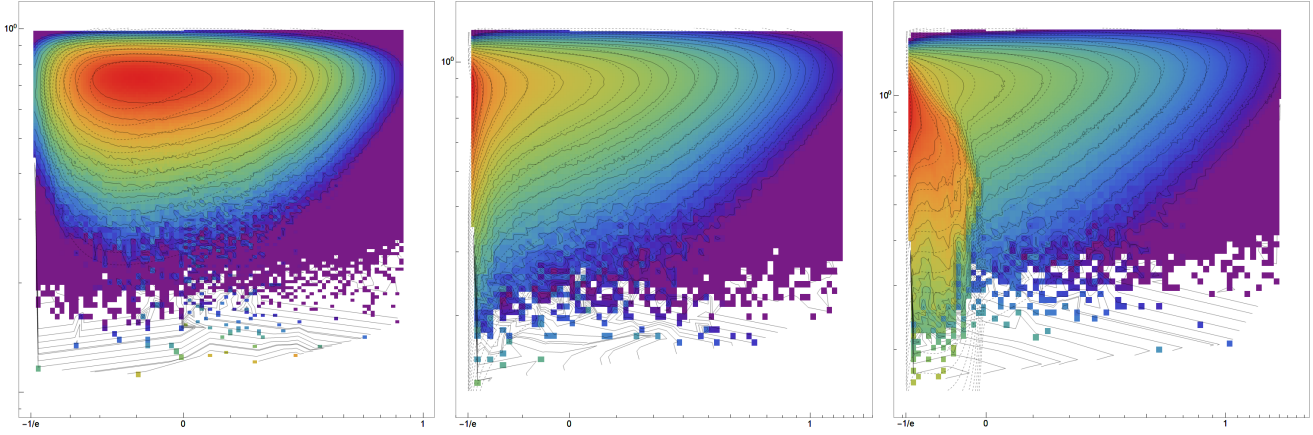


Figure 1: The joint distribution between thermal energy,  $E_T$  (horizontal), and kinetic energy  $E_K$  (vertical). Color shows the PDF computed from low resolution simulations, and ranges between 0 (purple) and 1 (red). The thermal energy develops a low  $E_T$  wall as well as a high  $E_T$  wing as the Mach number increases. We will improve the noise and accuracy of these fits, and probe if the deviation is numerical or physical.

### 2.1.1 Motivation: *turbulence*

The interstellar medium (ISM) is the gas between stars in the galaxy. It cools very effectively, so can be treated as isothermal (Krumholz 2014). The ISM is also turbulent, with supersonic shocks driven by supernovae causing supersonic turbulence throughout the interstellar medium (Elmegreen & Scalo 2004). This turbulence impacts the formation of stars (see Section 2.2) and causes a polarized screen that is blocking our view of the light from the big bang (see Section 2.3), among many other effects (Elmegreen & Scalo 2004). It is also interesting in its own right. We have developed analytic formulae for the probability density function (PDF) of internal energy and kinetic energy, as well as their joint distribution. In this project we will verify these formulae with high resolution simulations.

Supersonic turbulence is compressible, and the distribution of density fluctuations is described by a log normal, i.e. the log of density is distributed as a Gaussian (Vazquez-Semadeni 1994). The distribution of velocity is roughly Maxwellian, i.e. each of the three velocity components is a gaussian, and added in quadrature the distribution is Maxwellian. We have recently found analytic distributions for the internal energy and kinetic energy, as well as their joint distribution. (Rabatin et al 2022, in prep). Kinetic energy is defined in the familiar way,  $E_K = \frac{1}{2}\rho v^2$ . Internal energy is defined as  $E_T = c_s^2 \rho \ln \rho / \rho_0$ , where  $c_s$  is the sound speed and  $\rho_0$  is the mean density (Banerjee & Kritsuk 2018). The joint distribution of these two quantities can be seen in Figure 1, along with our analytic prediction (dotted lines). Each panel shows the joint PDF of  $E_K$  and  $E_T$ ; the color field shows the PDF derived from data; the solid lines show logarithmically spaced contours of the data; the dashed lines show the theoretical prediction. The first panel is subsonic, with  $M_S = 0.5$ , the middle has  $M_S = 1$ , and the third panel is slightly supersonic, with  $M_S = 2$ . Significant changes in the behavior of the distribution, with high  $K_E$  gas developing along side high  $E_T$  gas, are both predicted by the analytical dashed lines and seen in the data.

Our preliminary simulations were run with a modest resolution of  $256^3$ . This is enough to find reasonable agreement, but imperfect. This can be seen most easily in the first panel of Figure 1, by examining the center most (red) contours. The solid line shows simulation, while the dashed line shows theory, which clearly agrees, but only approximately. This lack of agreement can be one of several things, the first to examine is numerical resolution. With insufficient resolution, energy is transferred from large to small scales faster than would be natural, which could be why we have mediocre agreement in our predicted theory.

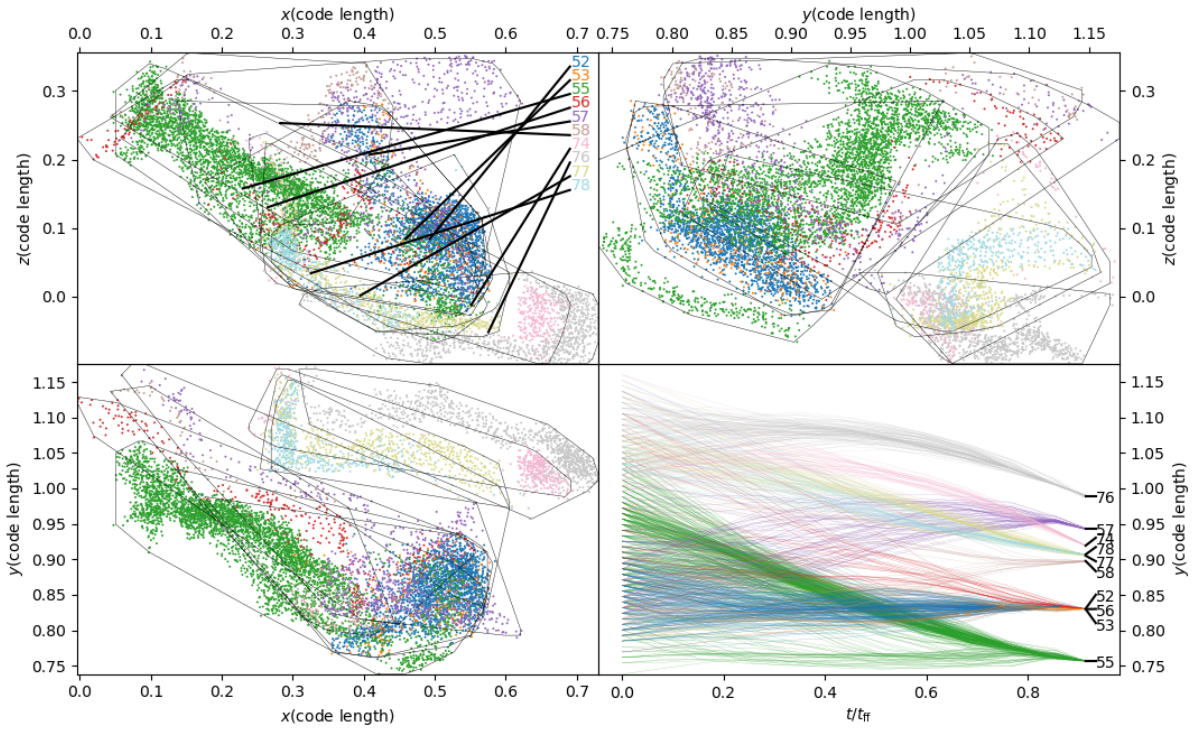


Figure 2: Stars form from chaotic molecular gas.

### 2.1.2 Simulations: *turbulence*

The proposed simulations will quadruple this resolution to  $1024^3$ . Owing to the substantial evolution with Mach number, we will run some subsonic cases ( $\mathcal{M}_S=0.5, 1.0$ ) and some moderate and highly supersonic cases ( $\mathcal{M}_S=2, 4, 7$ ). The turbulence is produced by adding a random velocity component to the field in a manner that slowly evolves over time (Schmidt et al. 2009). The simulations are run for  $5t_{dyn} = 0.5/\mathcal{M}_S$ , the dynamical time is the time it takes for the forcing pattern (half the box length) to cross the box. Running for  $5t_{dyn}$  allows the turbulence to be fully developed and statistically well sampled. These are dimensionless physics studies, so the box size and sound speed are unity.

## 2.2 Background: Star Formation

The formation of stars is filled with filamentary, fractal structures (André et al. 2014). The *cores* project will study the behavior of collapsing gas as it transitions from fractal structures to form dense prestellar cores. We will motivate the study in Section 2.2.1, and describe the simulations in 2.2.2.

### 2.2.1 Motivation: *cores*

The formation of stars is one of the most important processes in astrophysics, as stars provide most of the light we see in the night sky, and they produce the energy and metal that dictates the structure and composition of a galaxy. A *prestellar core* is a knot of dense gas formed by gravity in a molecular cloud, which will ultimately form a star. The formation of these cores is one of the more difficult puzzles in star formation, as it is fundamentally dictated by chaotic dynamics of the turbulence in the cloud. This is the focus of the *cores* project.

One of our previous studies (Collins et al 2022, in prep) examined the collapse of a molecular cloud by including semi-Lagrangian tracer particles that follow the flow. The particles that are found in dense cores at the end of the simulation are then followed backwards in time to examine the *preimage* of the gas, before it collapses. This will allow us to better constrain star formation models.

One of the curious findings is the fractal nature of the preimage gas. We find that gas from distinct cores at the end of the simulation begins life mixed with one another in a fractal manner. This can be seen in Figure 2, which shows the overlap of a collection of preimages at the beginning of the simulation in the first 3 panels, and the collapse to form dense cores in the fourth. The length scale in the first three panels translates to roughly 2 pc in size. These panels show the overlap and fractal, filamentary nature of the gas before it collapses. The last panel shows the un-mixing of the gas as it collapses in time.

### 2.2.2 Simulations: cores

The simulation presented in Figure 2 was one of a suite of three simulations with varied magnetic field strength. We began with fully developed turbulence, and then added tracer particles and turned on gravity and AMR. These simulations were relatively low resolution as we developed the analysis techniques and learned about extended nature of the primage gas. Our proposed simulations will greatly improve the resolution to explore if these structures are in fact fractal, or a result of low resolution. The size of the box is 5 pc, and the r.m.s. Mach number is 9. They will begin from existing simulation data. The target simulations will have  $512^3$  root grid and 4 levels of AMR, and  $1024^3$  particles. This is an increase of 4 in linear scale for the gas, and 16 for the particles over the results shown in Figure 2. The proposed suite of three simulations will mirror the magnetic field strengths of the preliminary studies. The simulations will be similar to those presented in (Collins et al. 2012), but with tracer particles and sinks. It will run for a total of one free-fall tiem, where  $t_{ff} = (G\rho)^{-1/2} = 1\text{Myr}$ . Here  $G$  is the gravitational constant, and  $\rho$  is the mean density of the box. These simulations will utilize isothermal MHD, gravity, and particle solvers.

## 2.3 Background: Foregrounds

The cosmic microwave background (CMB) is the light leftover from the creation of the universe. It has taught us a considerable amount about the structure, history, and future of the universe. To learn more from it, we must understand its polarization. To see the polarization of the CMB, we must first understand the polarization of the interstellar medium (ISM), which is much brighter and in the way. This project will perform simulations of driven magnetized turbulence, and compare the filamentary structure found with an analytic model of the CMB polarization developed by Huffenberger et al. (2020). We will motivate this project in Section 2.3.1, and describe the simulations we will perform in Section 2.3.2

### 2.3.1 Motivation: *foregrounds*

When the universe was very young, it was very small, and also very hot. So hot that everything was ionized. Sound waves left from the big bang travel through the universe, causing temperature fluctuations. Once the universe cooled enough, the electrons and protons combined to make the first Hydrogen. After this time, photons can travel great distances without running into an electron. These photons are the CMB. It is an extremely uniform 2.7K black body. Small ( $\mu K$ ) fluctuations in this temperature have been studied extensively by satellites such as Planck (Planck Collaboration et al. 2020). These fluctuations have answered many questions about the content and eventual fate of the universe. But there are still open questions.

Why is the CMB a single temperature? The universe is very large, and one side of the observable universe has never been in contact with the other. Given the expansion of the universe, one would expect significant fluctuations in temperature on the angular size of the full moon on the sky. One possible answer is an extremely rapid *inflation* of the universe, where the universe expands from the size of a proton to the size of the solar system within the first  $10^{-16}\text{s}$ . This is different from the *expansion* of the universe, which has been well established and a much more

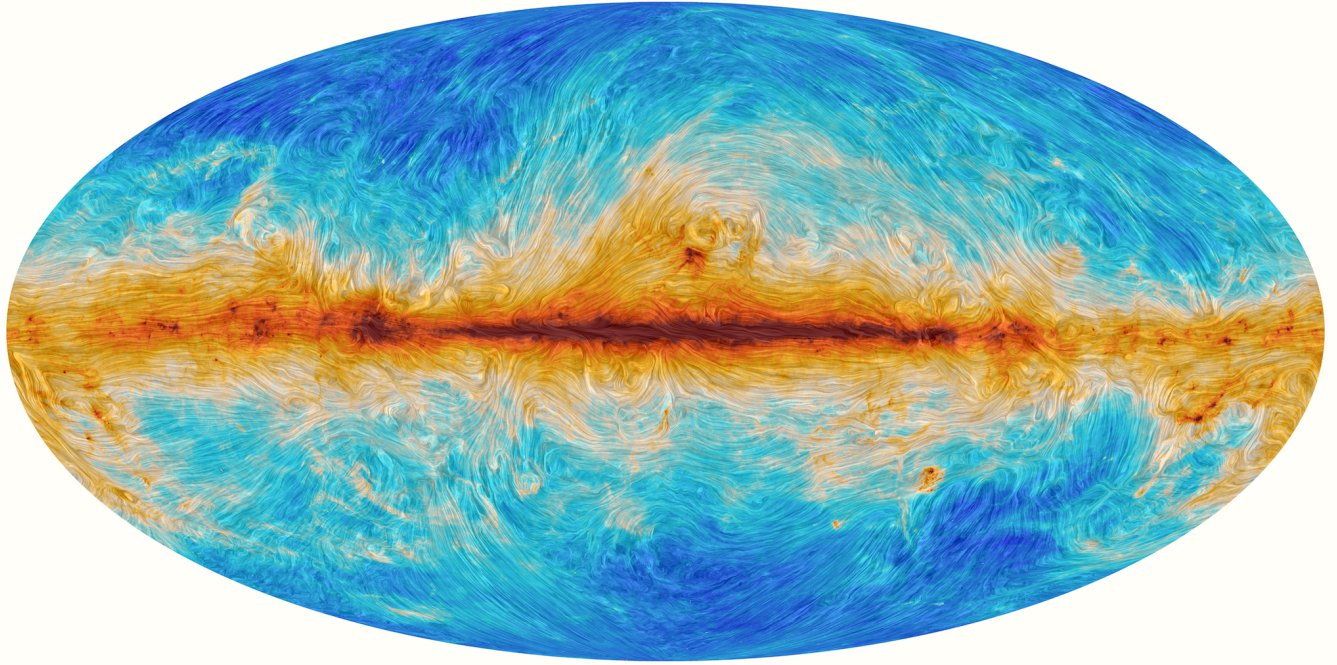


Figure 3: The large scale magnetic field of the galaxy as seen by the Planck satellite. The color field shows dust emission at 353GHz. The image is smeared along the direction of the magnetic field. ([Planck Collaboration et al. 2015](#))

leisurely pace. Such a rapid event would allow different patches of the universe to be at the same temperature very early on. It is also extraordinarily violent, would leave a sea of gravitational waves. These gravitational waves, being quadrupolar in nature, imprint a polarization on the CMB. To detect this polarization is to witness the violent birth of the Universe.

Unfortunately (for observing the CMB) the Galaxy we live in is filled with dust, which gives a polarized signal in the same frequency range as the polarized CMB. This dust, which includes iron and magnesium, lines up perpendicular to the magnetic field in the galaxy, not unlike iron filings around a bar magnet. These aligned grains radiate polarized thermal radiation in the microwave and infrared. This polarized signal is much brighter than the polarization in the CMB, so must be removed. In order to remove it, we must understand the statistical properties of the magnetic field in the Galaxy.

The Planck satellite ([Planck Collaboration et al. 2015](#)) measured the galactic magnetic field, and the result can be seen in Figure 3. Statistically, the polarization is described best by the quantities  $E$  and  $B$ . The  $E$ -mode is the amplitude of the polarized signal with polarization direction that is either parallel to or perpendicular to filamentary structures. The  $B$ -mode describes polarization at oblique angles. It is found that both structures are distributed over all scales in a power-law fashion, with  $E \propto k^{-2.35}$ , where  $k$  is wavenumber on the sky.  $B$  has a similar exponent but half the amplitude.

Our group has had success in reproducing similar polarized statistics in two settings; simulations of driven turbulence, and an analytic model based on magnetized filaments. In Stalpes et al 2022 (in prep) we demonstrated that MHD turbulence can reproduce similar exponents, with the value of the exponent and amplitude depending on velocity and magnetic field strength in the turbulence. In [Huffenberger et al. \(2020\)](#), we developed a model of the ISM polarization based on magnetized filaments. In this model, an ensemble of filaments is parametrized by their length, width, and the mean magnetic field angle to the filament. This ensemble, with the right parameters, can give a polarization signal that matches that of the sky. In the proposed simulations, we will combine these two approaches.

We will perform a series of driven turbulent boxes, as described in Section 2.1.2, but this time with magnetic fields. We will then use the filament finding tool DISPERSE ([Sousbie 2011](#)) to extract filamentary structure, and measure how well our analytic model reproduces the filament and polarization properties of the turbulent boxes.

The study done in Stalpes et al (2022, in prep) was a parameter sweep at moderate resolution ( $512^3$ ). These new simulations will be larger ( $1024^3$ ) and target Mach numbers that are higher than the previous family of simulations.

### 2.3.2 Simulations: *foregrounds*

Our previous simulations have indicated that, as far as the foregrounds are concerned, the ISM is most likely supersonic and super-Alfvénic. The primary parameters that dictate the behavior of the turbulence is the sonic Mach number,  $\mathcal{M}_S$ , and the AlfvénMach number,  $\mathcal{M}_A$ . These are the ratio of the r.m.s fluid speed to the sonic speed and Alfvén speed, respectively. The Alfvén speed is the speed a disturbance travels along a magnetic field in a plasma. As the character of the turbulence changes as both  $\mathcal{M}_S$  and  $\mathcal{M}_A$  are increased, we will perform a minimal 4 step parameter search, with  $\mathcal{M}_S$  and  $\mathcal{M}_A$  equal to 1 and 5. Thus,  $(\mathcal{M}_S, \mathcal{M}_A) = (1,1), (1,5), (5,1)$  and  $(5,5)$  alternately varying large and small field and velocity. These will use the MHD and driving modules in Enzo. We will increase the resolution beyond that of our preliminary runs, to  $1024^3$ . We will drive the turbulence for 5 dynamical times, where a dynamical time is the time for a typical driving pattern to cross the box. As the driving pattern is 1/2 the box,  $T_{dyn} = 0.5/\mathcal{M}_S$ . Driving for a number of dynamical times is important to develop statistically relaxed turbulence, as well as providing statistics for averaging.

## 2.4 Background: Galaxies

The galactic magnetic field can be seen in Figure 3, which shows the 353GHz channel of the Planck satellite. This figure shows an all-sky projection of dust in the galaxy, smeared along the direction of the magnetic field. Our goal in the *galaxies* project is to understand the origin of this magnetic field. We will discuss the background in Section 2.4.1, and describe the simulations we will perform in Section 2.4.2

### 2.4.1 Motivation: *galaxies*

The Milky Way has a large scale magnetic field of roughly  $\sim 5\mu\text{G}$ , about 200,000 time weaker than a refrigerator magnet, but spanning the entire galaxy. In the previous project, *foregrounds*, the goal is to remove the magnetic field in the sky, while in the *galaxies* project the goal is to form the magnetic field.

The origin of this magnetic field is an open question. There are presently two known *dynamics*, that is mechanisms to amplify magnetic fields. They differ in two ways; the length scales over which they act, and the time scales over which they act. The fast dynamo converts turbulent kinetic energy to magnetic energy at small scales, and produces disordered fields quickly. The slow dynamo produces large scale fields slowly, with large scale convective motions. The magnetic field in the Milky Way, as well as other similar galaxies, shows large scale order, but based on observations of old galaxies, must have been built up quickly.

The magnetic field in the Galaxy is largely in one direction, closely following the spiral arms. Both dynamo mechanisms produce a substantial amount of field in all directions. Thus to have a field of mostly one direction, the other directions must be expelled from the galaxy. (Selectively damping out one component of magnetic field is not possible at these scales.) Thus the buoyancy of the gas as it leaves the face of the disk is important in setting the rate of growth of the mean field. Like many problems in physics, the answer depends sensitively on boundary conditions.

The circum-galactic medium (CGM) is the gas that's outside disk the galaxy, but still bound to it. It is extremely hot (millions of Kelvin) and extremely low density ( $0.1 \text{ cm}^{-3}$ ) and thus unfortunately difficult to observe. The purpose of this project is to examine the impact of the circum-galactic medium (CGM) properties on the dynamo. We expect that an ordered field within the disk requires a buoyant CGM, so that gas that is expelled from the galaxy by supernovae continues to rise, rather than falling back down immediately.

### 2.4.2 Simulations: *galaxies*

The disk of our simulated galaxies will be 500pc thick and 25kpc in radius. Our proposed simulation domain will begin at very large scale, 1.3 Mpc. This is to separate the boundary from the region of interest, and to give the CGM a large enough volume to expand. This will begin at  $256^3$ , much smaller than the other simulations, but this suite of galaxy simulations has much deeper AMR. We will resolve a nest of refinement grids, each one 1/2 of its parent grid on a side, giving constant number of zones per level. This will be done for 5 levels. We will allow the simulation to refine for a further 4 levels, based on the local density of the gas. Nine levels then gives us 10pc of resolution on the finest level, so we will resolve molecular clouds by a few zones. We will have ample resolution in the disk to study the dynamo action as it occurs, and sufficient resolution in the CGM to serve as an appropriate boundary. As we are simulating the entire galaxy, we can no longer use an idealized isothermal equation of state as the other simulations do, but will use ISM heating and cooling functions by way of the tabulated look up using Grackle (Smith et al. 2017). We will perform four such simulations with a variety of models for the CGM. One simulation will have a buoyant CGM, one will not, and the other two are developmental simulations for defining simulation parameters. Simulations will last for 1Gyr, several orbital timescales for the galaxy.

These simulations will also be useful in conjunction with the *foregrounds* project. The two approaches compliment each other, as the *foregrounds* simulations will resolve the turbulence with great detail, but the *galaxies* simulations will capture the multiphase nature of the ISM and the large scale morphology.

## 3 Computational Method

For the proposed simulations, we will use Enzo (Bryan et al. 2014; Collins et al. 2010). Enzo is an adaptive mesh refinement (AMR) code, which dynamically adds resolution elements as the simulation evolves. (Magneto)hydrodynamics is solved on an Eulerian grid using finite volume techniques. Specifically, for hydrodynamics we use the piecewise parabolic method (Colella & Woodward 1984), and we use a piecewise linear method for MHD (Li et al. 2008). The AMR uses the scheme of Berger & Colella (1989), and the MHD uses the scheme of Balsara (2001). Gravity is solved with fast Fourier transforms on the root grid, and multi-grid relaxation on the sub-grid patches (Bryan et al. 2014). The *turbulence*, *cores*, and *foregrounds* simulations use an isothermal equation of state. Heating and cooling for the *galaxies* simulations will be handled with the package Grackle (Smith et al. 2017). Turbulent driving in the *turbulence* and *foregrounds* simulations will be done by adding a large-scale random velocity field at every time step, with the velocity field evolving using an Ornstein-Uhlenbeck process (Schmidt et al. 2009).

## 4 Simulation Plan

Here we will outline the simulations to be performed for each of the projects.

The total cost for one simulation is determined by multiplying the cost for a single zone-update by the number of zones and the number of updates:

$$SU = SU_{zu} N_Z N_U, \quad (1)$$

where  $SU$  is the total cost,  $SU_{zu}$  is cost in  $SU$ -per-zone-update,  $N_Z$  is the number of zones, and  $N_U$  is the number of updates.  $SU_{zu}$  is determined by the total time for one time step using 64 cores per node. Overhead and imperfect scaling is accounted for in  $SU_{zu}$  by performing simulations that use the target physics packages, resolution, appropriate AMR structures.  $SU_{zu}$  changes for each suite as the physics packages involved are different, and the overhead from the AMR hierarchy is different. More details on the calculation of  $SU_{zu}$  can be seen in the Scaling document.

The choice of physics packages for each suite is motivated in Section 2, and the measurement of  $SU_{zu}$  is presented in the Scaling and Performance document.

The estimate of the number of zones,  $N_Z$ , is determined by the target resolution for the simulation. For the fixed resolution simulations, this is simply the number of zones. For the AMR simulations, the actual number of zones

created is a product of the chaotic processes in the system. For these we use approximate the covering fraction with previous simulations.

The number of updates,  $U$ , is found as  $U = T/\Delta T$ , where the total simulation time is  $T$  and the size of the timestep is  $\Delta T$ .  $T$  is determined by the physics problem. The size of the time step  $\Delta T$  is determined by a standard Courant condition, that is a wave cannot cross half of one zone in a timestep,

$$\Delta T = \eta \frac{\Delta x}{v_{\text{signal}}}, \quad (2)$$

and  $\eta < 0.5$ . We determine  $v_{\text{signal}} = c_s + v_{\max}$  as the sum of the sound speed and the max velocity, from preliminary studies, and then use use Equation 2 to determine the number of steps on each level.

Both the *turbulence* and *foregrounds* simulations are fixed resolution and employ only the random forcing physics package. The former will use the hydro solver PPM, and the later will use our MHD solver, which has a slightly higher cost. Both will be run at  $1024^3$ . The total time,  $T$ , is 5 shock-crossing times, so  $T = 5L/M_S$ , where  $L$  is the size of the driving pattern. The timestep,  $\Delta T$ , also decreases with Mach number as Equation 2, and is determined measuring the signal speed  $v_{\text{signal}}$  from previous fully developed turbulence simulations and rescaling with the Mach number.

The timing for the *cores* and *galaxies* suite is done in an identical manner, but the number of zones  $N_Z$  is now dynamically determined by the portion of the flow that is turning into stars. This is a chaotic process, so formally impossible to predict. However, it can be expected to be roughly similar to previous simulations, so we estimate the covering fraction from those. The timestep per level is typically half that of the level above, so we estimate the signal speed from previous simulations and estimate the timestep for each level with Equation 2. The number of zones on a level is found as

$$N_Z = \frac{V f_\ell}{\Delta x_\ell^3}, \quad (3)$$

where  $V$  is the total volume for each simulation,  $f_\ell$  is the volume fraction on level  $\ell$ , and  $\Delta x_\ell$  on each level is 1/8th that of its parent.

The *cores* simulations will have  $512^3$  root grid zones and  $1024^3$  particles, as well as 4 levels of AMR. The refinement will be based on the density. It will use the isothermal MHD solver, the gravity solver, and the particle update machinery. The net cost per zone update for this combination of physics solvers and a similar AMR structure to the production simulations is discussed in the Scaling document, and seen in the  $SU_{zu}$  column of Table 2. We will perform three of these simulations.

The *galaxies* suite will restrict the dynamic AMR to the disk of the galaxy, and use a tower of refinement, with each level 1/2 the length of the parent, to separate the outer part of the CGM at 1.3 Mpc from the small star forming regions in the disk. The first 5 levels will be static nested AMR levels, the final 4 will be dynamic. For each level we approximate that about 10% coverage of the parent level. This is by construction for the first 5, and from experience with similar simulations for the final 4. These simulations will use the MHD solver, the gravity solver, the particle machinery for the star particles, heating and cooling of the gas, and supernovae feedback. We have performed a preliminary simulation using 5 levels to determine the cost per timestep,  $SU_{zu}$ , and anticipated signal speed,  $v_{\text{signal}}$ , to determine the timestep size. The results can be seen in Table 2.

Table 2 shows the breakdown of the total request by simulation. The *turbulence* and *foregrounds* suites are itemized by Mach number, while the *cores* and *galaxies* suites are itemized by AMR level. Shown in that table is the name; the parameter, either Mach number, level, or Sonic and Alfvén Mach numbers; the volume fraction; the number of zones  $N_Z$ ; the total simulation time  $T$ ; the timestep size  $\Delta T$ ; the total number of updates  $N_U$ , the cost per update given the AMR and physics usage,  $SU_{zu}$ ; and finally the total SU cost.

The disk usage is also estimated from the number of zones,  $N_Z$ . Each zone stores a number of fields,  $N_F$ : 5 for *turbulence*(density, 3 velocity, and energy); 14 for *cores* and *foregrounds*(density, energy, 3 velocity, 3 magnetic fields, 3 electric fields, 3 additional magnetic fields, see [Collins et al. \(2010\)](#)); 24 for the *galaxies* suite (14 for MHD,

10 for additional chemistry fields.) So the total memory is 8 bytes for all of  $N_Z N_F$  fields. It is listed in Gb in the table.

## 5 Access to Other Computational Resources

**Local Computing Environment** The astrophysics group at Florida State University has a small cluster with 300 cores. This machine is useful for testing and debugging, but not large enough for the proposed simulations. Florida State University also maintains a research cluster, but it is also insufficient for this research.

**Other supercomputing resources.** The PI of the current proposal does not presently have access to other supercomputing resources.

## 6 Personnel

The PI of this project is Dr. David C. Collins, an Associate Professor in the Florida State University Department of Physics. Dr. Collins has more than fifteen years of experience working using high performance computing platforms for research in computational astrophysics. He is also a lead developer of the code Enzo, which has a long history of simulation success.

Three PhD students will be working on the projects. Luz Jimenez Vela will be responsible for the *cores* project. Branislav Rabatin is responsible for both the *turbulence* and *foregrounds* projects. Jacob Strack is responsible for the *galaxies* project.

## References

- André, P., Di Francesco, J., Ward-Thompson, D., Inutsuka, S. I., Pudritz, R. E., & Pineda, J. E. 2014, in Protostars and Planets VI, ed. H. Beuther, R. S. Klessen, C. P. Dullemond, & T. Henning, 27
- Balsara, D. S. 2001, J. Comput. Phys, 174, 614
- Banerjee, S. & Krtsuk, A. G. 2018, Phys. Rev. E, 97, 023107
- Berger, M. J. & Colella, P. 1989, J. Comput. Phys, 82, 64
- Bryan, G. L., Norman, M. L., O’Shea, B. W., Abel, T., Wise, J. H., Turk, M. J., Reynolds, D. R., Collins, D. C., Wang, P., Skillman, S. W., Smith, B., Harkness, R. P., Bordner, J., Kim, J.-h., Kuhlen, M., Xu, H., Goldbaum, N., Hummels, C., Krtsuk, A. G., Tasker, E., Skory, S., Simpson, C. M., Hahn, O., Oishi, J. S., So, G. C., Zhao, F., Cen, R., Li, Y., & Enzo Collaboration. 2014, ApJS, 211, 19
- Colella, P. & Woodward, P. R. 1984, J. Comput. Phys, 54, 174
- Collins, D. C., Krtsuk, A. G., Padoan, P., Li, H., Xu, H., Ustyugov, S. D., & Norman, M. L. 2012, ApJ, 750, 13
- Collins, D. C., Xu, H., Norman, M. L., Li, H., & Li, S. 2010, ApJS, 186, 308
- Elmegreen, B. G. & Scalo, J. 2004, ARA&A, 42, 211
- Huffenberger, K. M., Rotti, A., & Collins, D. C. 2020, ApJ, 899, 31
- Krumholz, M. R. 2014, Phys. Rep., 539, 49
- Li, S., Li, H., & Cen, R. 2008, ApJS, 174, 1

Table 2: Allocation request. Cost for each simulation,  $SU$ , is computed from the cost per zone-update,  $SU_{zu}$ , the number of zones  $N_Z$ , and the number of timesteps  $N_U$ . For the *turbulence* and *foregrounds* suites, the simulations are itemized by Mach number and Alfvén Mach number,  $M_s$  and  $M_a$ , which affect the total time,  $T$ , and timestep size  $\Delta T$ . The cost of the AMR simulations, *cores* and *galaxies* is estimated for each level,  $\ell$ , by estimating the volume fraction,  $f_\ell$ , covered on level  $\ell$ , time step  $\Delta t$ . Long term disk usage is estimated as  $N_Z$  times the number of fields for each simulation. More details are given in the text

suite	$M_s$	$f_\ell$	$N_Z$	$T$	$\Delta T$	$N_U$	$SU_{zu}$	$SU$
<i>turbulence</i>	0.5	1	$1.1 \times 10^9$	5.0	$7 \times 10^{-6}$	$7.0 \times 10^5$	$2.0 \times 10^{-11}$	$1.5 \times 10^4$
<i>turbulence</i>	1.0	1	$1.1 \times 10^9$	2.5	$5 \times 10^{-6}$	$4.7 \times 10^5$	$2.0 \times 10^{-11}$	$1.0 \times 10^4$
<i>turbulence</i>	2.0	1	$1.1 \times 10^9$	1.3	$4 \times 10^{-6}$	$3.5 \times 10^5$	$2.0 \times 10^{-11}$	$7.6 \times 10^3$
<i>turbulence</i>	4.0	1	$1.1 \times 10^9$	0.6	$2 \times 10^{-6}$	$2.9 \times 10^5$	$2.0 \times 10^{-11}$	$6.3 \times 10^3$
<i>turbulence</i>	7.0	1	$1.1 \times 10^9$	0.4	$1 \times 10^{-6}$	$2.7 \times 10^5$	$2.0 \times 10^{-11}$	$5.8 \times 10^3$
							SU	$4.5 \times 10^4$
							Disk	$5.6 \times 10^3$
suite	$\ell$	$f_\ell$	$N_Z$	$T$	$\Delta T$	$N_U$	$SU_{zu}$	$SU$
<i>cores</i>	0	$1.0 \times 10^0$	$1.3 \times 10^8$	1 Myr	$5 \times 10^{-3}$ Myr	$2.2 \times 10^2$	$6.3 \times 10^{-11}$	$1.8 \times 10^0$
<i>cores</i>	1	$4.6 \times 10^{-1}$	$4.9 \times 10^8$	1 Myr	$2 \times 10^{-3}$ Myr	$4.4 \times 10^2$	$6.3 \times 10^{-11}$	$1.4 \times 10^1$
<i>cores</i>	2	$8.3 \times 10^{-2}$	$7.1 \times 10^8$	1 Myr	$1 \times 10^{-3}$ Myr	$8.7 \times 10^2$	$6.3 \times 10^{-11}$	$3.9 \times 10^1$
<i>cores</i>	3	$1.3 \times 10^{-2}$	$8.7 \times 10^8$	1 Myr	$6 \times 10^{-4}$ Myr	$1.7 \times 10^3$	$6.3 \times 10^{-11}$	$9.5 \times 10^1$
<i>cores</i>	4	$1.8 \times 10^{-3}$	$1.0 \times 10^9$	1 Myr	$3 \times 10^{-4}$ Myr	$3.5 \times 10^3$	$6.3 \times 10^{-11}$	$2.2 \times 10^2$
							per sim	$3.7 \times 10^2$
							SU	$1.1 \times 10^3$
							Disk	$2.0 \times 10^4$
suite	$M_{s,a}$	$f_\ell$	$N_Z$	$T$	$\Delta T$	$N_U$	$SU_{zu}$	$SU$
<i>foregrounds</i>	1,1	1	$1.1 \times 10^9$	3	$4 \times 10^{-5}$	$6.9 \times 10^4$	$6.2 \times 10^{-11}$	$4.6 \times 10^3$
<i>foregrounds</i>	1,5	1	$1.1 \times 10^9$	3	$1 \times 10^{-5}$	$2.1 \times 10^5$	$6.2 \times 10^{-11}$	$1.4 \times 10^4$
<i>foregrounds</i>	5,1	1	$1.1 \times 10^9$	0.6	$1 \times 10^{-5}$	$4.2 \times 10^4$	$6.2 \times 10^{-11}$	$2.8 \times 10^3$
<i>foregrounds</i>	5,5	1	$1.1 \times 10^9$	0.6	$9 \times 10^{-6}$	$6.9 \times 10^4$	$6.2 \times 10^{-11}$	$4.6 \times 10^3$
							SU	$2.6 \times 10^4$
							Disk	$1.7 \times 10^4$
suite	$\ell$	$f_\ell$	$N_Z$	$T$	$\Delta T$	$N_U$	$SU_{zu}$	$SU$
<i>galaxies</i>	0	$1.0 \times 10^0$	$1.7 \times 10^7$	1 Gyr	$4 \times 10^{-4}$ Gyr	$2.8 \times 10^3$	$3.0 \times 10^{-10}$	$1.4 \times 10^1$
<i>galaxies</i>	1	$1.0 \times 10^0$	$1.3 \times 10^8$	1 Gyr	$2 \times 10^{-4}$ Gyr	$5.7 \times 10^3$	$3.0 \times 10^{-10}$	$2.3 \times 10^2$
<i>galaxies</i>	2	$1.2 \times 10^{-1}$	$1.3 \times 10^8$	1 Gyr	$9 \times 10^{-5}$ Gyr	$1.1 \times 10^4$	$3.0 \times 10^{-10}$	$4.5 \times 10^2$
<i>galaxies</i>	3	$2.9 \times 10^{-2}$	$2.5 \times 10^8$	1 Gyr	$4 \times 10^{-5}$ Gyr	$2.3 \times 10^4$	$3.0 \times 10^{-10}$	$1.7 \times 10^3$
<i>galaxies</i>	4	$4.2 \times 10^{-3}$	$2.9 \times 10^8$	1 Gyr	$2 \times 10^{-5}$ Gyr	$4.5 \times 10^4$	$3.0 \times 10^{-10}$	$3.9 \times 10^3$
<i>galaxies</i>	6	$3.9 \times 10^{-4}$	$1.7 \times 10^8$	1 Gyr	$6 \times 10^{-6}$ Gyr	$9.1 \times 10^4$	$3.0 \times 10^{-10}$	$9.4 \times 10^3$
<i>galaxies</i>	9	$3.9 \times 10^{-5}$	$8.8 \times 10^7$	1 Gyr	$7 \times 10^{-7}$ Gyr	$1.8 \times 10^5$	$3.0 \times 10^{-10}$	$3.9 \times 10^4$
							per sim	$5.4 \times 10^4$
							SU	$2.2 \times 10^5$
							Disk	$2.2 \times 10^4$
							SU	$2.9 \times 10^5$
							Disk	$6.4 \times 10^4$

Planck Collaboration, Ade, P. A. R., Aghanim, N., Alina, D., Alves, M. I. R., Armitage-Caplan, C., Arnaud, M., Arzoumanian, D., Ashdown, M., Atrio-Barandela, F., Aumont, J., Baccigalupi, C., Banday, A. J., Barreiro, R. B., Battaner, E., Benabed, K., Benoit-Lévy, A., Bernard, J. P., Bersanelli, M., Bielewicz, P., Bock, J. J., Bond, J. R., Borrill, J., Bouchet, F. R., Boulanger, F., Bracco, A., Burigana, C., Butler, R. C., Cardoso, J. F., Catalano, A., Chamballu, A., Chary, R. R., Chiang, H. C., Christensen, P. R., Colombi, S., Colombo, L. P. L., Combet, C., Couchot, F., Coulais, A., Crill, B. P., Curto, A., Cuttaia, F., Danese, L., Davies, R. D., Davis, R. J., de Bernardis, P., de Gouveia Dal Pino, E. M., de Rosa, A., de Zotti, G., Delabrouille, J., Désert, F. X., Dickinson, C., Diego, J. M., Donzelli, S., Doré, O., Douspis, M., Dunkley, J., Dupac, X., Efstathiou, G., Enßlin, T. A., Erikson, H. K., Falgarone, E., Ferrière, K., Finelli, F., Forni, O., Frailis, M., Fraisse, A. A., Franceschi, E., Galeotta, S., Ganga, K., Ghosh, T., Giard, M., Giraud-Héraud, Y., González-Nuevo, J., Górski, K. M., Gregorio, A., Gruppuso, A., Guillet, V., Hansen, F. K., Harrison, D. L., Helou, G., Hernández-Monteagudo, C., Hildebrandt, S. R., Hivon, E., Hobson, M., Holmes, W. A., Hornstrup, A., Huffenberger, K. M., Jaffe, A. H., Jaffe, T. R., Jones, W. C., Juvela, M., Keihänen, E., Keskitalo, R., Kisner, T. S., Kneissl, R., Knoche, J., Kunz, M., Kurki-Suonio, H., Lagache, G., Lähteenmäki, A., Lamarre, J. M., Lasenby, A., Lawrence, C. R., Leahy, J. P., Leonardi, R., Levrier, F., Liguori, M., Lilje, P. B., Linden-Vørnle, M., López-Caniego, M., Lubin, P. M., Macías-Pérez, J. F., Maffei, B., Magalhães, A. M., Maino, D., Mandolesi, N., Maris, M., Marshall, D. J., Martin, P. G., Martínez-González, E., Masi, S., Matarrese, S., Mazzotta, P., Melchiorri, A., Mendes, L., Mennella, A., Migliaccio, M., Miville-Deschénes, M. A., Moneti, A., Montier, L., Morgante, G., Mortlock, D., Munshi, D., Murphy, J. A., Naselsky, P., Nati, F., Natoli, P., Netterfield, C. B., Noviello, F., Novikov, D., Novikov, I., Oxborrow, C. A., Pagano, L., Pajot, F., Paladini, R., Paoletti, D., Pasian, F., Pearson, T. J., Perdereau, O., Perotto, L., Perrotta, F., Piacentini, F., Piat, M., Pietrobon, D., Plaszczynski, S., Poidevin, F., Pointecouteau, E., Polenta, G., Popa, L., Pratt, G. W., Prunet, S., Puget, J. L., Rachen, J. P., Reach, W. T., Rebolo, R., Reinecke, M., Remazeilles, M., Renault, C., Ricciardi, S., Riller, T., Ristorcelli, I., Rocha, G., Rosset, C., Roudier, G., Rubiño-Martín, J. A., Rusholme, B., Sandri, M., Savini, G., Scott, D., Spencer, L. D., Stolyarov, V., Stompor, R., Sudiwala, R., Sutton, D., Suur-Uski, A. S., Sygnet, J. F., Tauber, J. A., Terenzi, L., Toffolatti, L., Tomasi, M., Tristram, M., Tucci, M., Umana, G., Valenziano, L., Valiviita, J., Van Tent, B., Vielva, P., Villa, F., Wade, L. A., Wandelt, B. D., Zacchei, A., & Zonca, A. 2015, *A&A*, 576, A104

Planck Collaboration, Aghanim, N., Akrami, Y., Ashdown, M., Aumont, J., Baccigalupi, C., Ballardini, M., Banday, A. J., Barreiro, R. B., Bartolo, N., Basak, S., Battye, R., Benabed, K., Bernard, J. P., Bersanelli, M., Bielewicz, P., Bock, J. J., Bond, J. R., Borrill, J., Bouchet, F. R., Boulanger, F., Bucher, M., Burigana, C., Butler, R. C., Calabrese, E., Cardoso, J. F., Carron, J., Challinor, A., Chiang, H. C., Chluba, J., Colombo, L. P. L., Combet, C., Contreras, D., Crill, B. P., Cuttaia, F., de Bernardis, P., de Zotti, G., Delabrouille, J., Delouis, J. M., Di Valentino, E., Diego, J. M., Doré, O., Douspis, M., Ducout, A., Dupac, X., Dusini, S., Efstathiou, G., Elsner, F., Enßlin, T. A., Erikson, H. K., Fantaye, Y., Farhang, M., Fergusson, J., Fernandez-Cobos, R., Finelli, F., Forastieri, F., Frailis, M., Fraisse, A. A., Franceschi, E., Frolov, A., Galeotta, S., Galli, S., Ganga, K., Génova-Santos, R. T., Gerbino, M., Ghosh, T., González-Nuevo, J., Górski, K. M., Gratton, S., Gruppuso, A., Gudmundsson, J. E., Hamann, J., Handley, W., Hansen, F. K., Herranz, D., Hildebrandt, S. R., Hivon, E., Huang, Z., Jaffe, A. H., Jones, W. C., Karakci, A., Keihänen, E., Keskitalo, R., Kiiveri, K., Kim, J., Kisner, T. S., Knox, L., Krachmalnicoff, N., Kunz, M., Kurki-Suonio, H., Lagache, G., Lamarre, J. M., Lasenby, A., Lattanzi, M., Lawrence, C. R., Le Jeune, M., Lemos, P., Lesgourgues, J., Levrier, F., Lewis, A., Liguori, M., Lilje, P. B., Lilley, M., Lindholm, V., López-Caniego, M., Lubin, P. M., Ma, Y. Z., Macías-Pérez, J. F., Maggio, G., Maino, D., Mandolesi, N., Mangilli, A., Marcos-Caballero, A., Maris, M., Martin, P. G., Martinelli, M., Martínez-González, E., Matarrese, S., Mauri, N., McEwen, J. D., Meinhold, P. R., Melchiorri, A., Mennella, A., Migliaccio, M., Millea, M., Mitra, S., Miville-Deschénes, M. A., Molinari, D., Montier, L., Morgante, G., Moss, A., Natoli, P., Nørgaard-Nielsen, H. U., Pagano, L., Paoletti, D., Partridge, B., Patanchon, G., Peiris, H. V., Perrotta, F., Pettorino, V., Piacentini, F., Polastri, L., Polenta, G., Puget, J. L., Rachen, J. P., Reinecke, M., Remazeilles, M., Renzi, A., Rocha, G., Rosset, C., Roudier, G., Rubiño-Martín, J. A., Ruiz-Granados, B., Salvati, L., Sandri, M., Savelainen, M., Scott, D., Shellard, E. P. S., Sirignano, C., Sirri, G., Spencer, L. D., Sunyaev, R., Suur-Uski, A. S., Tauber, J. A., Tavagnacco, D., Tenti, M.,

Toffolatti, L., Tomasi, M., Trombetti, T., Valenziano, L., Valiviita, J., Van Tent, B., Vibert, L., Vielva, P., Villa, F., Vittorio, N., Wandelt, B. D., Wehus, I. K., White, M., White, S. D. M., Zacchei, A., & Zonca, A. 2020, A&A, 641, A6

Schmidt, W., Federrath, C., Hupp, M., Kern, S., & Niemeyer, J. C. 2009, A&A, 494, 127

Smith, B. D., Bryan, G. L., Glover, S. C. O., Goldbaum, N. J., Turk, M. J., Regan, J., Wise, J. H., Schive, H.-Y., Abel, T., Emerick, A., O'Shea, B. W., Anninos, P., Hummels, C. B., & Khochfar, S. 2017, MNRAS, 466, 2217

Sousbie, T. 2011, MNRAS, 414, 350

Vazquez-Semadeni, E. 1994, ApJ, 423, 681